Alexandria Engineering Journal (2015) 54, 281–293

HOSTED BY

Alexandria University

Alexandria Engineering Journal

www.elsevier.com/locate/aej
www.sciencedirect.com

ORIGINAL ARTICLE

Heat transfer due to impinging double free circular jets

Mohamed A. Teamah [a,*,1], Mohamed M. Khairat [b]

[a] Faculty of Engineering and Technology, Arab Academy for Science and Technology and Maritime Transport, Alexandria, Egypt
[b] Faculty of Engineering, Suez Canal University, Ismailia, Egypt

Received 27 March 2015; revised 10 May 2015; accepted 18 May 2015
Available online 9 June 2015

KEYWORDS

Heat transfer;
Free impingement jets;
Hydraulic jump;
Super cooling

Abstract The heat transfer and fluid flow between a horizontal heated plate and impinging circular double jets were studied experimentally. The parameters investigated are the Reynolds number of each jet and jet-to-jet spacing. Experiments are carried out covering a range for Reynolds number from 7100 to 30,800 for each jet, the dimensionless jet-to-jet spacing from 22.73 to 90.1. During experimental phases, the right jet Reynolds number was higher than the left jet Reynolds number. The isothermal contours were plotted for different cases as well as the distribution of water film thickness over the heated plate. The results indicated that increasing the Reynolds number of one jet than the other increases both local and average Nusselt numbers. In addition, increasing the jet-to-jet spacing at the same Reynolds number increases the average Nusselt number.

1. Introduction

Impinging cooling is an effective way to generate super cooling rate in many engineering applications such as steel, glass, quenching and paper industries. Impinging jets are used to cool down the products after rolling. Also, it is used in laser or plasma cutting processes and cooling of electronic equipment. Firstly, in 1964 Watson [1] studied analytically the motion of the thin layer formed when a smooth jet of water falls vertically on a horizontal plane and spread out radially. In the same year Chaudhury [2] studied the heat transfer to Watson's analysis in a similar manner. In 1981 Craik et al. [3] measured the liquid depth using a light absorption technique in which a laser shone through water containing a strong dye. Liquid depths ahead and behind the jump were determined as well as the depth profiles of the jump in the stable regime. In 1991 Vader et al. [4] measured the heat flux distribution and the surface temperature on a flat, upward facing, constant heat flux surface cooled by a planar, impinging water jet. Jet velocities were between 1.8 and 4.5 m/s, fluid temperatures of 30, 40 and 50 °C and heat fluxes between 0.25 and 1.00 MW/m^2. In 1988 Zeiton [5] studied the fluid flow and the heat transfer between a horizontal plate and a single liquid circular jet impinging. A theoretical analysis was performed and the flow pattern was obtained. The results included the film thickness distribution at both sides of hydraulic jump and the determination of the position of the hydraulic jump and the velocity distribution within the film. Experiments were also conducted for comparing with the results of theoretical analysis. To visualize the jet nature, it divides the area near-

* Corresponding author.
[1] On leave "Mechanical Engineering Department, Faculty of Engineering, Alexandria University, Egypt".
Peer review under responsibility of Faculty of Engineering, Alexandria University.

http://dx.doi.org/10.1016/j.aej.2015.05.010

Nomenclature

A	area of segments, m^2
CNC	computerized numerical control
Cp	specific heat, J/kg K
d_j	jet diameter, m
h	local heat transfer coefficient, W/m^2 K
h_{avr}	local average heat transfer coefficient, W/m^2 K
$\overline{h}$	average heat transfer coefficient, W/m^2 K
H	thickness of water film, m
k	fluid thermal conductivity, W/m K
Nu	local Nusselt number, hd_j/k
Nu_{avr}	average local Nusselt number, $h_{avr}d_j/k$
$\overline{Nu}$	average Nusselt number, $\overline{h}d_j/k$
m	water mass flow rate (kg/s)
Re	Reynolds number, Vd_j/v
Re_L	Reynolds number of the left jet, Vd_j/v
Re_R	Reynolds number of the right jet, Vd_j/v
R	radial coordinate, m
Pr	Prandtl number, $\mu Cp/k$
PVC	polyvinyl chloride
T_s	wall temperature, K
T_w	water temperature, K
V	jet velocity, m/s
X	distance between two jets, m

Greek symbols

v	kinetic fluid viscosity, m^2/s
ρ	fluid density, kg/m^3
μ	dynamic fluid viscosity, kg/m s
σ	surface tension, N/m

Subscripts

n	number of segment

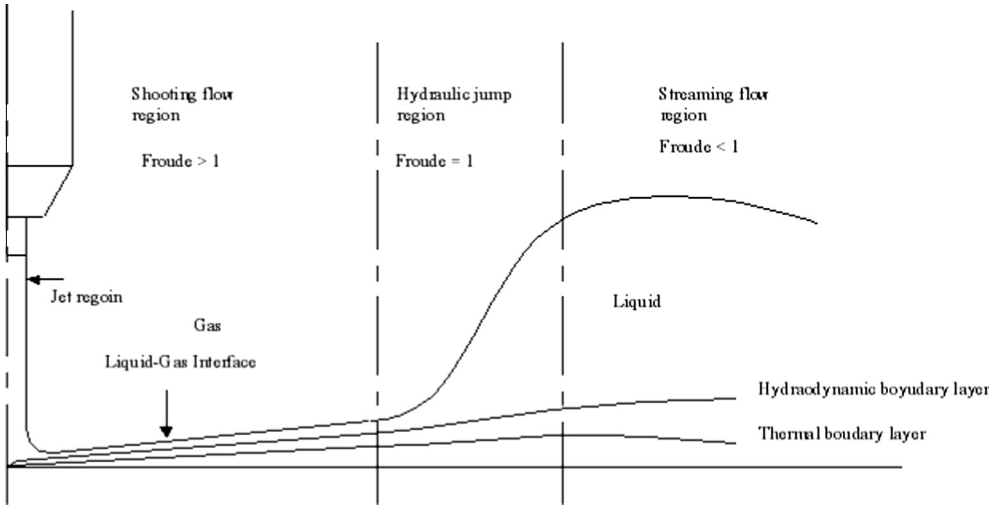

Figure 1 Hydraulic jet nature.

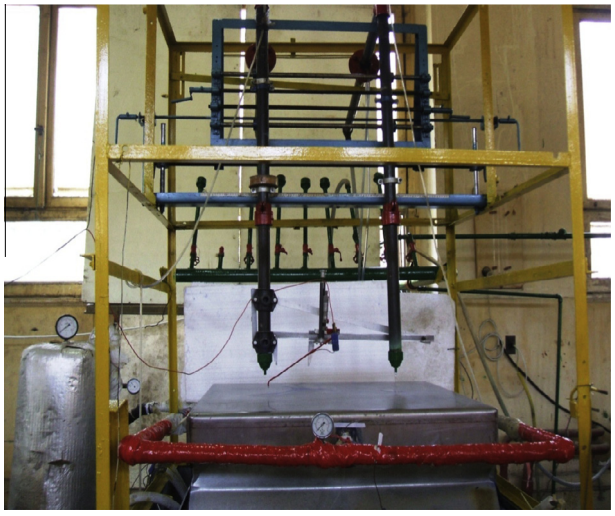

Figure 2 Experimental test rig details.

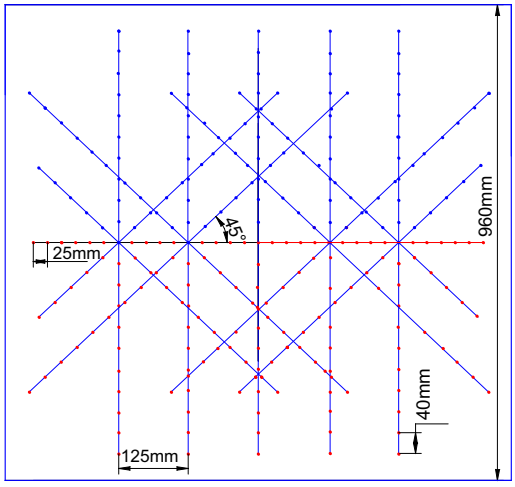

Figure 3 Distribution for thermocouple over the heated plate.

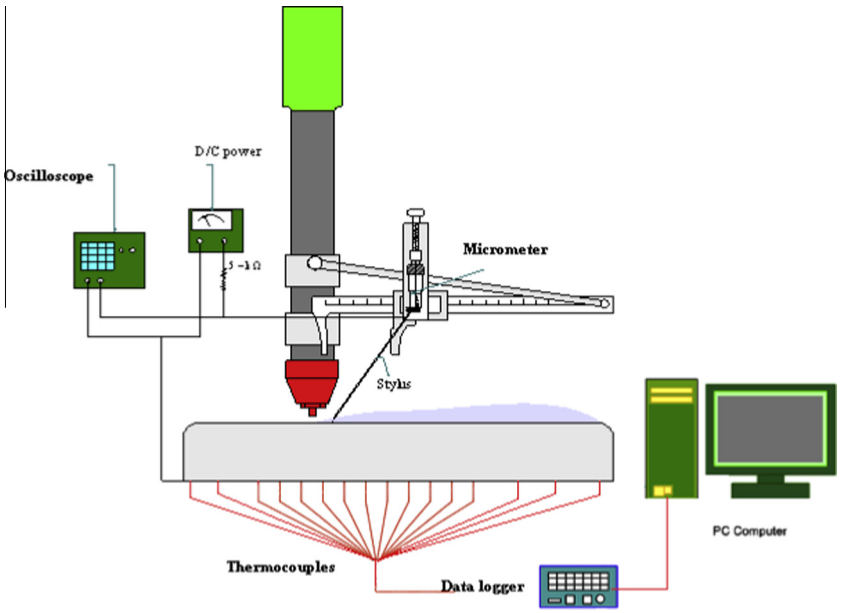

Figure 4 Details construction for measuring the film thickness.

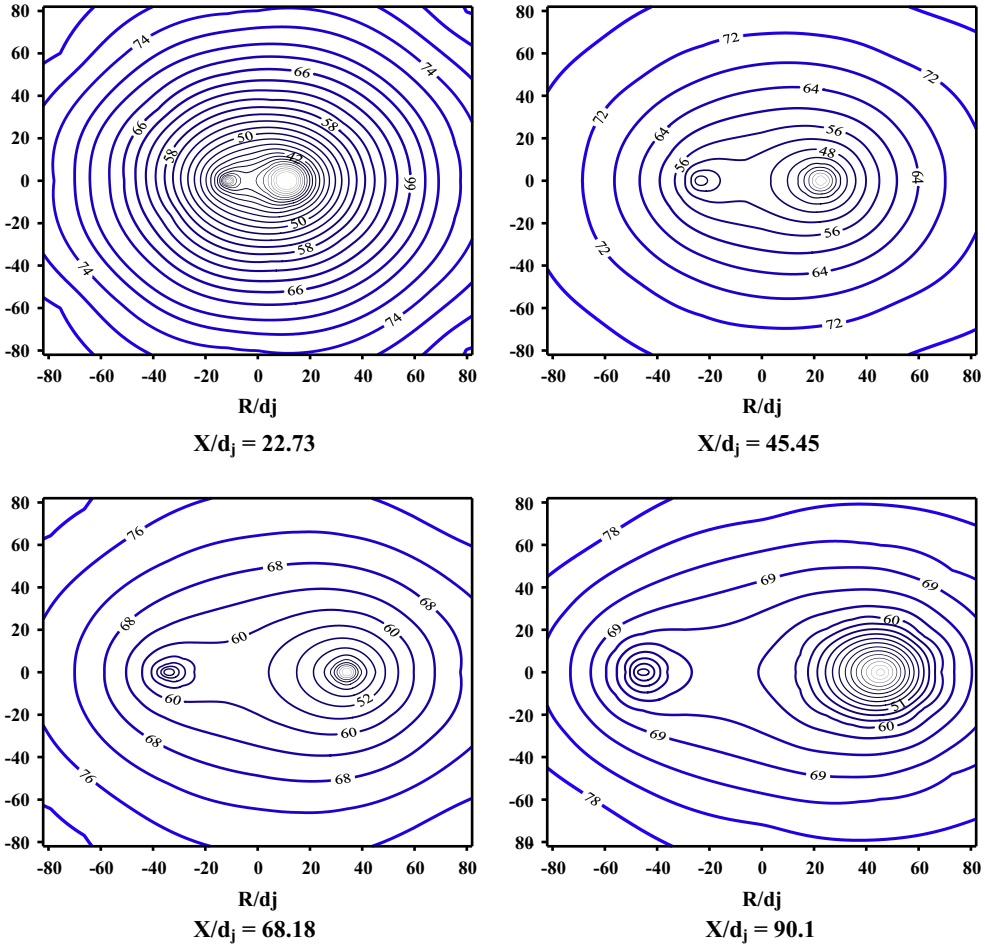

Figure 5 Effect of spacing distance on surface temperature distribution for Re_L = 7100 and Re_R = 15,400.

by into 3 regions: the shooting flow region (Froude > 1) where the liquid–gas interface nearly adheres to both thermal and hydrodynamic boundary layers, the hydraulic jump region (Froude = 1) where the liquid–gas interface gradually deviates from both layers and streaming flow region (Froude < 1) where the liquid–gas interface is greatly deviated from both layers. This can be manifested in Fig. 1.

In 2003 and 2006 Teamah and Farahat [6,7] studied the heat transfer and flow due to the impingement of a circular jet on a horizontal heated surface numerically and experimentally for single jet and experimentally only for multi jets of four arrangements, double jets, three in line, L-shaped and full cluster, in order to study the effect of the interaction between the jets on heat transfer. The water volume flow rates 1, 5 and 8 l/min per jet are used for multi jets. It was found for multi jets that the interaction between the jets leads to reduce the mean velocity of the fluid film, which in turn leads to reduce both the local and the average local Nusselt number compared to single jet. The overall average Nusselt number for multi jet is higher than single jet of one jet of the multi jets. In 2004 Wang et al. [8] studied the heat transfer due to jet impinging experimentally using integrated heater devices and temperature sensors. In 2003 Fabbri et al. [9] focused on circular arrays of free surface micro jets. Experiments were conducted by employing three jet pitches 1, 2 and 3 mm and four jet diameters 50, 100,150 and 250 μm and two different fluids. The jet Reynolds number range was varied between 90 and 2000 while the Prandtl number varied from 6 to 84. They found that Nusselt number improves by increasing the jet Reynolds number and Prandtl number. In 1991 Stevens and Webb [10,11] studied the effect of jet inclination on the local heat transfer under an obliquely impinging, round; free liquid jet striking a constant heat flux surface investigated experimentally. They studied the effect of jet Reynolds number in the range 6600–52,000, and jet inclination ranging from 40 to 90°.

In 2006 Gradeck et al. [12] studied experimentally a free impinging axisymmetric jet on a moving surface. A power relation has been derived for calculating the radius of the jump as a function of Reynolds number and Webber number. In 2001 Chen et al. [13] studied the heat transfer in free surface liquid jet impingement with magneto-fluid coating on the heated surface. Slayzak et al. [14] studied the local convection, heat transfer coefficient distributions along a constant heat flux surface experiencing impingement by two, planner, and free surface jets of water. Lienhard [15] studied the use of water jet array on removing heat fluxes of 1–17 MW/m^2 over an area of 10 cm^2. The jet array consists of 14 tube nozzles. The jet array speed of 46.5 m/s produces a heat transfer coefficient measured to be 220,000 W/m^2 K at the stagnation point. In 1998 Sun et al. [16] worked to conduct an extensive and consistent study

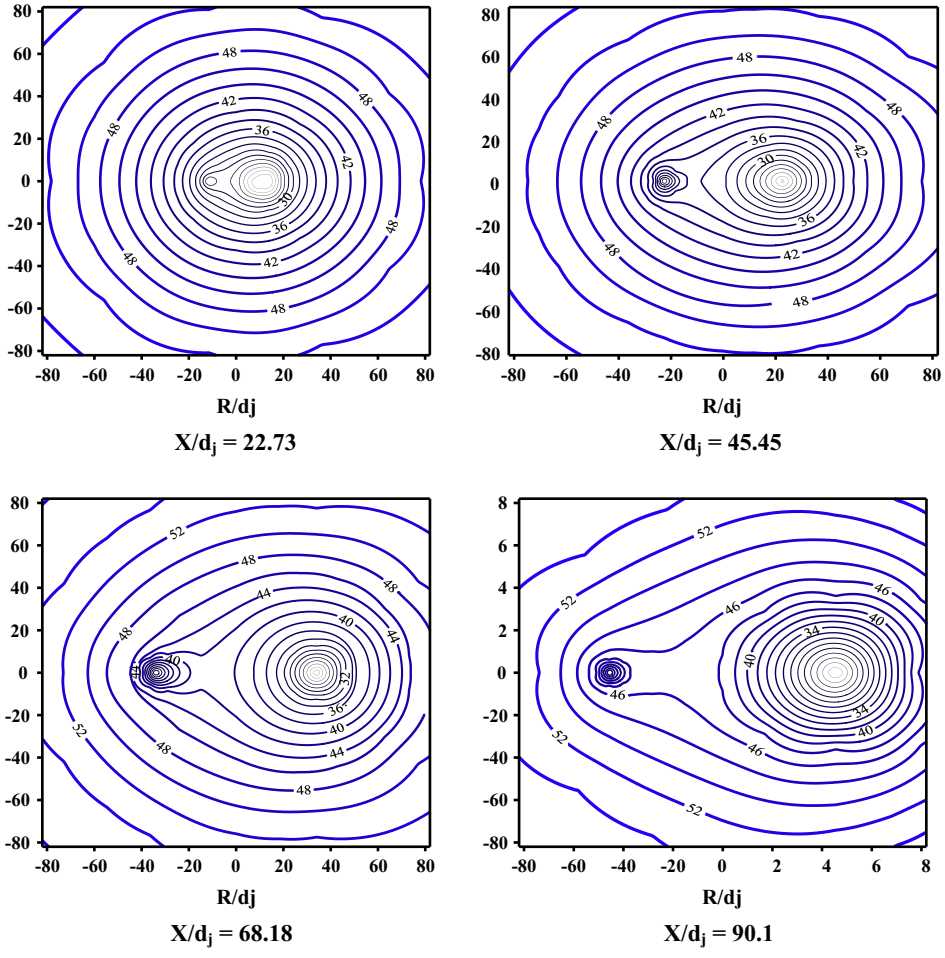

Figure 6 Effect of spacing distance on surface temperature distribution for Re_L = 7100 and Re_R = 23,150.

using three test liquids to testify the effect of Prandtl number on the local heat transfer for free surface circular jets. Local measurements were made to investigate the characteristic of convective heat transfer from small heaters to circular jets. Wang et al. [17] studied the conjugate heat transfer between a laminar free impinging liquid jet and a laterally insulated disk with arbitrary temperature or heat flux distribution prescribed on the non-impinged surface analytically. The heat transfer coefficient between the jet and the solid disk was influenced by the Prandtl number of the fluid, the ratio of the fluid conductivity to the solid conductivity and the ratio of the thickness to the radius of the disk, as well as the prescribed temperature or heat flux profile.

Measurements were made in 1997 by Ma et al. [18] to investigate the local behavior of the recovery factor and the heat transfer coefficient with the free surface circular jets. The experiments were performed with the transformer oil jets impinging on a vertical constant heat flux surface from a small pipe and orifice nozzles. In 1991 Stevens and Webb [11] investigated characterized local heat transfer coefficients for round, single-phase free liquid jets impinging normally against a flat uniform heat flux surface. The local Nusselt number characteristic is found to be dependent on nozzle diameter. In 1977 Ishigai et al. [19] studied the hydrodynamic and heat transfer characteristics of two domains of the jet flow. The first domain is the jump region and the other is the interfering films of two equal jets. The film of the jet flow was measured and analyzed. Recently Teamah et al. [20] studied the effect of inclined free liquid jet on the film thickness. More recently, Malvandi et al. [21] studied the thermodynamics optimization for fluid flow over isothermal plate. Also Das [22] studied the flow and heat transfer characteristics using nanofluid. And Hayat et al. [23] studied unsteady stagnation point. Then Nasif et al. [24] did simulation of jet impingement over rotating disk.

From the previous review the effect of interaction of the jets stream on both heat transfer and film jump was not examined. The present work is devoted to study the effect of interaction of the jets stream on the heat transfer coefficient by changing the strength of one or both jets, as well as changing the space between the two jets.

2. Experimental apparatus

Fig. 2 shows the experimental test rig. It is composed of water circuit. It is designed for providing the jets and the steam generator with water. The water circuit consists of: storage tank, header tank, collecting tank and water jets.

The storage tank dimensions are of 150 cm long × 100 cm wide × 100 cm depth. The storage tank is fed from the main

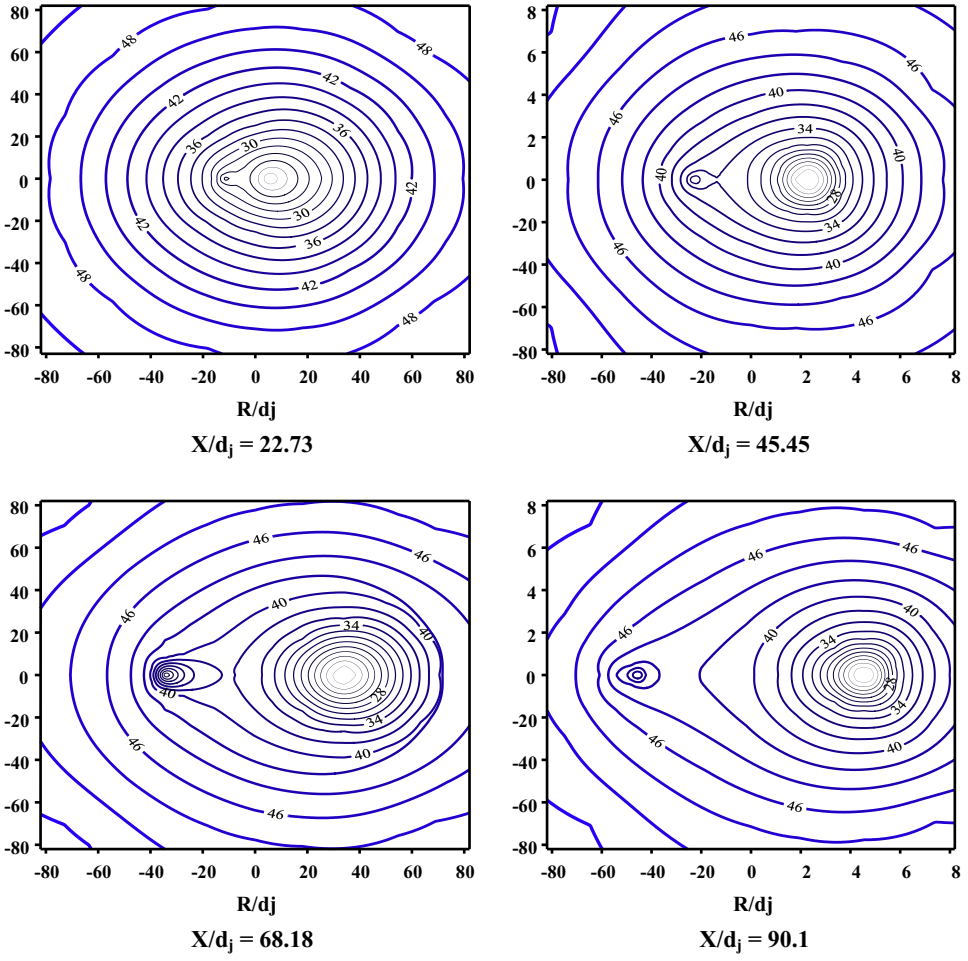

Figure 7 Effect of spacing distance on surface temperature distribution for Re_L = 7100 and Re_R = 30,800.

source through a gate valve. The storage tank is equipped with suitable overflow and drain pipes. The water inside the storage tank is delivered to the header tank through a circulating pump. The header tank is a cylindrical shape of dimensions 90 cm diameter and 100 cm height to insure the required static head, the header tank was placed at a level above the heated plate by 10 m. The header tank has an auxiliary feed from the main source. It provides continuous flow with a constant water head. The water flows down by Gravity from header tank to the distribution pipe. Two pipes are connected to the distribution pipe, each pipe is provided with a gate valve, orifice plate and nozzle. The gate valve regulates the flow rate and the orifice measures the volumetric flow rate of water. The discharge coefficient of the orifice plate is calculated from the equation developed by White [25]:

$$C_d = 0.60062 + 16.21219\mathrm{Re}^{-0.75} \quad (1)$$

The water falls from the nozzle onto the heated plate and spreads out rapidly to its outer edge. The falling water from the plate is collected in a collecting tank.

The second circuit is the steam circuit. It consists of a steam generator fed by water from the storage tank through a pump. The steam generator is provided with three immersed electrical heaters. Each heater is 220 V and 6 kW capacities. The steam is superheated by throttling. The steam is distributed into two branches as it is supplied to the heating chamber from four points. The heating chamber is a box with dimensions of $90 \times 90 \times 15$ cm. It is made of stainless steel of thickness 4 mm and open top side. The bottom side of the heating chamber has a few inclinations toward the center of the base to prevent the settling of the condensation inside the heating chamber. Pressure gauges and thermocouples are used to measure the pressure and temperature of the steam before entering the heating chamber. A perforated box is placed inside the heating chamber in order to provide good distribution of the steam inside the heating chamber. At the center of the base of the heating chamber a drain pipe is fitted. Two layers of asbestos and glass wool are used to insulate the heating chamber. The heating chamber is covered by a stainless steel plate of 6 mm thickness. This thickness is capable of avoiding sagging of the plate due to steam pressure. Thermocouples are located on the back of the plate to measure the wall temperature. The mechanical mechanism is designed to provide the PVC pipes with two-dimensional movements. The first movement is vertically upwards or downwards as to study the effect of distance between the jet and plate. The second movement is longitudinal to change the distance between the two jets with respect to each other.

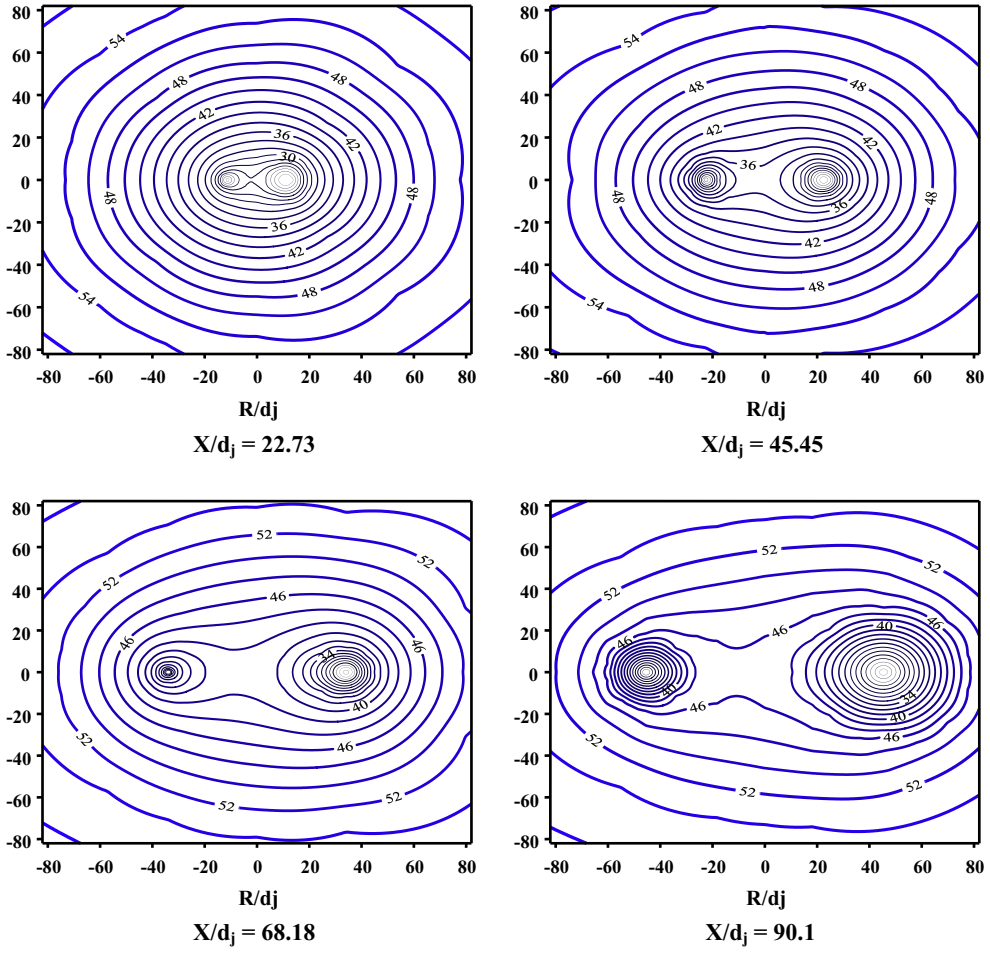

Figure 8 Effect of spacing distance on surface temperature distribution for Re_L = 15,400 and Re_R = 23,150.

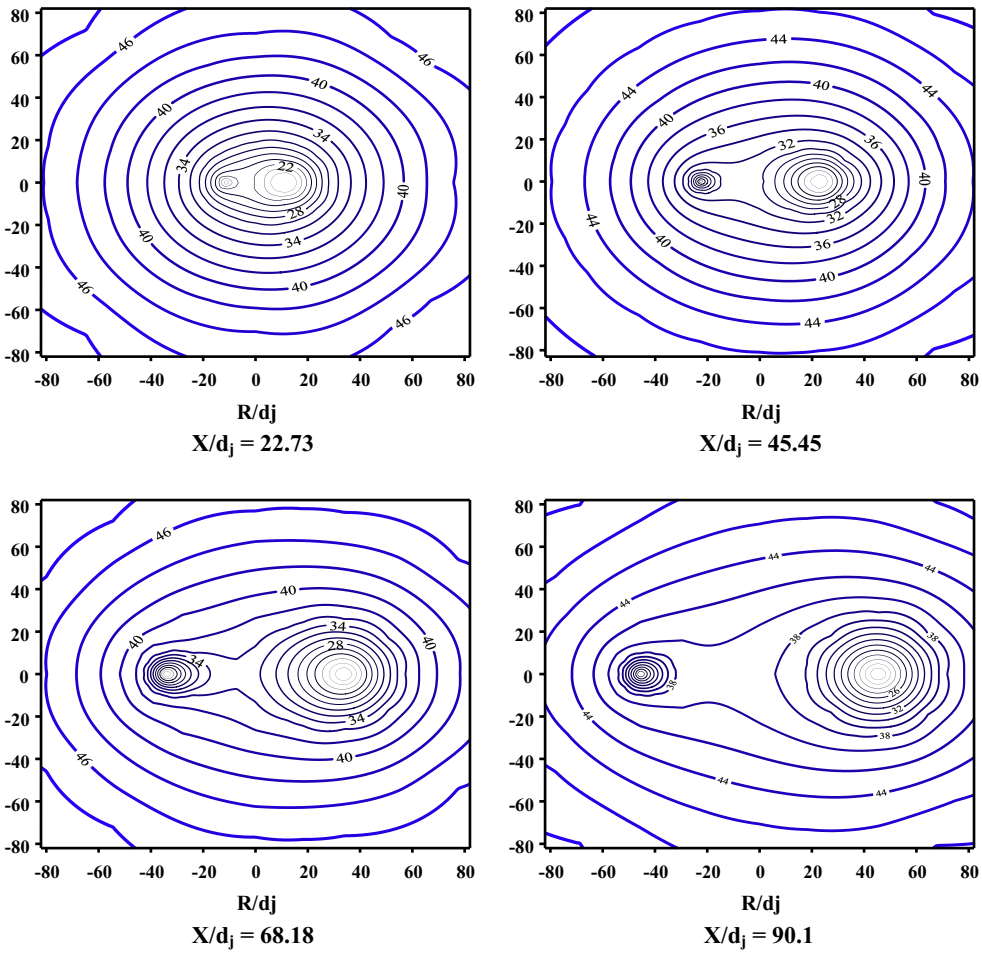

Figure 9 Effect of spacing distance on surface temperature distribution for Re_L = 15,400 and Re_R = 30800.

3. The measuring techniques

3.1. The wall temperature

The measurements of water film temperature are needed to determine the local Nusselt number and therefore the average local Nusselt number. The average local Nusselt number is an indicator for the average value of Nusselt number for the area swept from the jet to the studied point. The thermocouples distribution over the back of the horizontal plate is shown in Fig. 3. The total numbers of thermocouples are 273 thermocouples of *T* type. Each thermocouple is inserted into a drilled hole in the stainless steel plate. This hole is at a depth of 3 mm and diameter 2 mm using CNC to ensure exact accuracy for the spacing between thermocouples. The thermocouples are fixed in these holes by copper oxide cement. The thermocouples are connected to temperature reading out (Model SR630). A computer program is designed to read and log-out all the measurements. The accuracy of the temperature reading is 0.05 °C.

3.2. Measuring the water film thickness

The details of water film thickness measurement are shown in Fig. 4. A micrometer of 0.01 mm sensitivity is used for measuring the film thickness. A vernier caliper connected to PVC pipe with two clamps around the PVC pipe. This whole mechanism allows to measure the film thickness at different radius from the jet and different circumference. A special electrical circuit is used. This circuit is manufactured from a D/C power supply of 5 V, 5 kΩ resistance connected in series with power supply and an oscilloscope. The oscilloscope is used for showing the position of the stylus with respect to the film thickness. At the beginning of the experiments, the stylus is in the air above the water film. In this case the electric circuit is open and the oscilloscope is supposed to read the 5-volt. If the micrometer is turned and the stylus touches the free surface of water, at this condition the electric circuit will be closed and the oscilloscope reading will drop. At the beginning of experiment the set point is logged when the stylus touches the horizontal plate, and then the stylus moves away from the plate; after that water flows during operation and the stylus moves toward the heated plate and when it touches the water the circuit is closed and the reading is logged. The difference between this reading and the set point gives the film thickness and the process is further repeated.

3.3. Measuring the temperature of water film

The same mechanical mechanism is used for measuring the water film thickness and is also used to determine the temperature of water over the surface. The water film temperature is

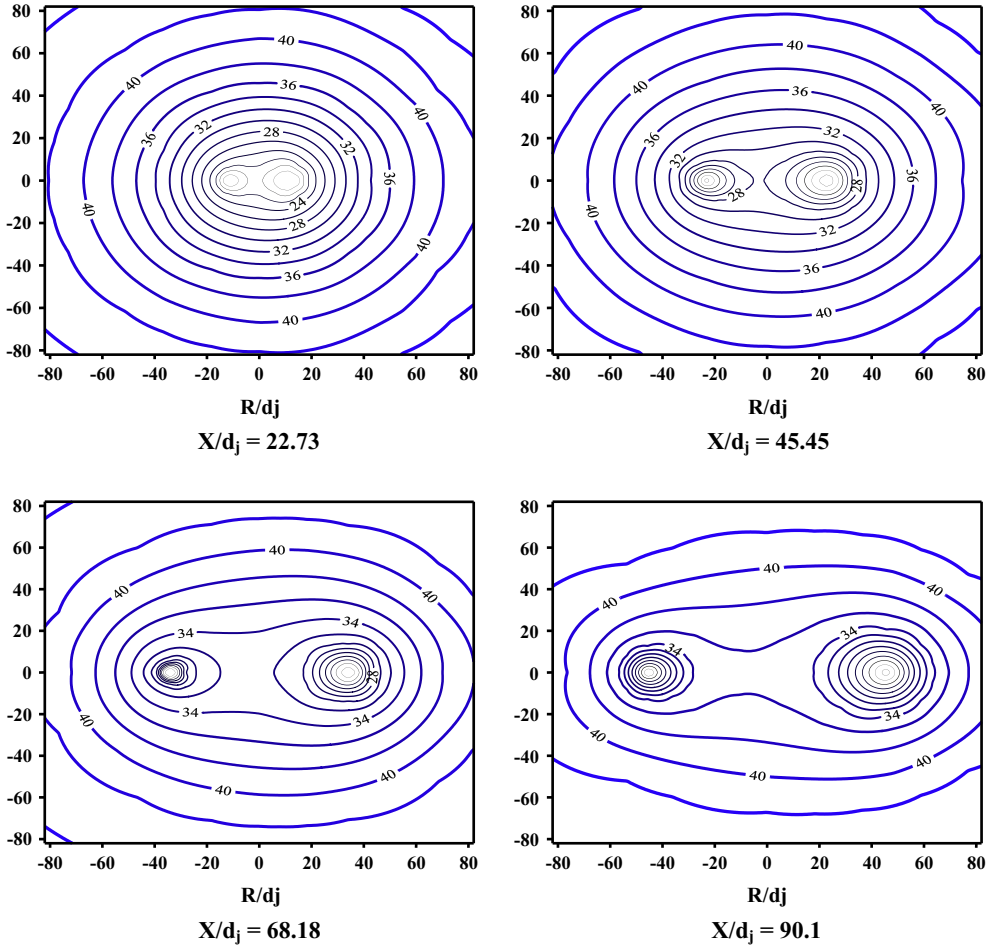

Figure 10 Effect of spacing distance on surface temperature distribution for Re_L = 23,150 and Re_R = 30,800.

measured at different radius. The stylus is connected to the temperature read out.

4. Data reduction

4.1. Local and average local heat transfer coefficient

For the determination of the local heat transfer for double jet heat balance is performed. The thermal energy is absorbed by the flowing film equal to the heat transferred from the hot plate to the film. The readings of the plate temperatures and their positions are compiled to Win surf computer program, which draws the isothermal wall temperature over the plate. The isothermals are complied with AutoCAD program. The wall temperature distribution around the center of the plate is divided into segments. These segments were divided at interval of 1 °C. The heat balance is made for the segment of the plate to the water film. The area of this segment is calculated with AutoCAD program.

The heat balance for the segment is as follows:

$$mCp(T_{wn} - T_{wn-1}) = A_n h_n (T_{sn} - T_{wn}) \tag{2}$$

The average local heat transfer is determined from the integration of the local heat transfer coefficient between the areas.

4.2. Local and average local Nusselt number

The local Nusselt number of segment could be determined as following:

$$\mathrm{Nu}_n = \frac{h_n d_j}{k} \tag{3}$$

where k, is the thermal conductivity of water at the water temperature over the segment T_f

$$T_f = \frac{\frac{T_{wn}+T_{wn+1}}{2} + T_s}{2} \tag{4}$$

The average local Nusselt number is determined as follows:

$$\mathrm{Nu}_{\mathrm{avr}} = \frac{h_{\mathrm{avr}} d_j}{k} \tag{5}$$

The average Nusselt number is determined as follows:

$$\overline{\mathrm{Nu}} = \frac{\bar{h} d_j}{k} \tag{6}$$

5. Experimental uncertainty analysis

The uncertainty in the data calculation was based on ANSI/ASME reported by Holman 1994. The uncertainty calculation method used involves calculating derivatives of the

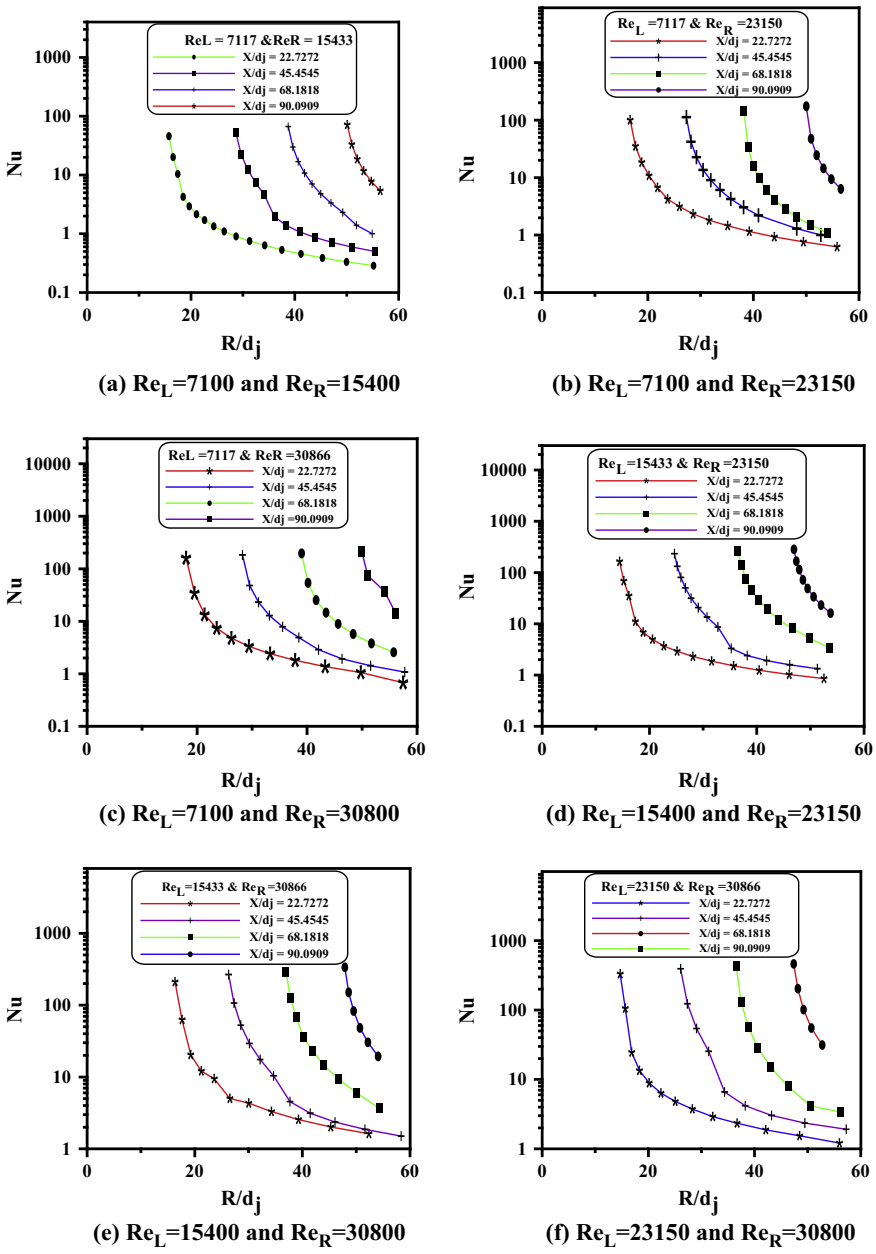

Figure 11 Effect of interaction spacing on local Nusselt number.

desired variable with respect to individual experimental quantities and applying known uncertainties. The magnitude of the uncertainty is estimated from Eq. (7)

$$w_R = \sqrt{\left[\left(\frac{\partial R}{\partial x_1}w_1\right)^2 + \left(\frac{\partial R}{\partial x_2}w_2\right)^2 + \left(\frac{\partial R}{\partial x_3}w_3\right)^2 + \cdots + \left(\frac{\partial R}{\partial x_n}w_n\right)^2\right]} \tag{7}$$

The accuracy of the thermocouples is within $\pm 0.1\,^{\circ}C$. The uncertainty of the manometers is estimated to be 4%. The maximum uncertainties of dimensionless parameters were $\pm 8\%$ for Reynolds number, $\pm 10\%$ for Nusselt number and $\pm 6\%$ for water film thickness.

6. Results and discussions

6.1. Effect of jet spacing on isothermal contours

The effect of jet spacing on the temperature distribution was shown from Figs. 5–10. For all experiments, the jet of low Reynolds number is on the left side. It observed from the figures that the isothermals look like the two sources flow. Each source is represented by one jet. Near each jet the isothermals appear as concentric circles whose centers are the jets position. In the jet area, the isothermals are close to each other. This leads to a high heat transfer rate at this area. As we move away from the jet area, the circular shape for the isothermals is converted to an oval shape. As well as the spacing between the

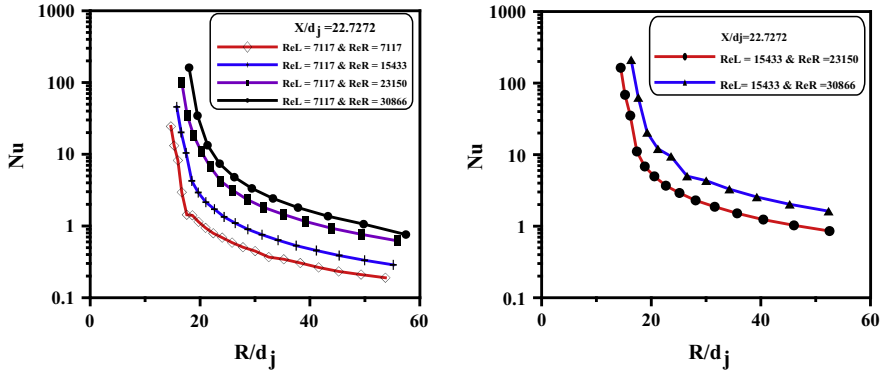

(a) $Re_L = 7100$ (b) $Re_L = 15400$

Figure 12 Effect of Reynolds number on local Nusselt number.

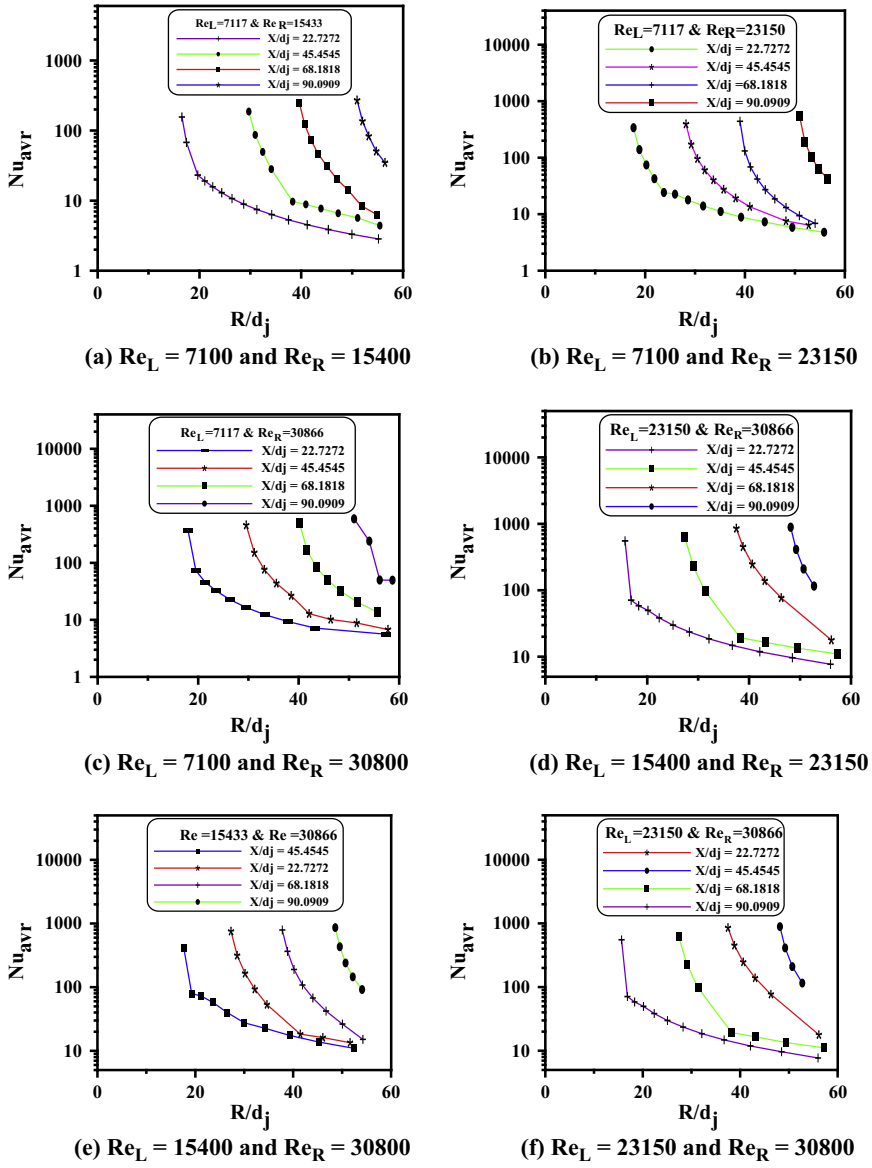

(a) $Re_L = 7100$ and $Re_R = 15400$ (b) $Re_L = 7100$ and $Re_R = 23150$

(c) $Re_L = 7100$ and $Re_R = 30800$ (d) $Re_L = 15400$ and $Re_R = 23150$

(e) $Re_L = 15400$ and $Re_R = 30800$ (f) $Re_L = 23150$ and $Re_R = 30800$

Figure 13 Effect of interaction spacing on average local Nusselt number.

isothermals is increased. This means the heat transfer rate is lower than the previous area. Each jet represents one focus for the oval shape. The major axis of the oval shape is concurrent to the line passing by the two jets. The line passing by the two jets is the axis of symmetry for the isothermals. Also it is shown, a large oval isothermal contours bounded the two oval shapes. In a small distance between jets, the jet areas are small compared with that for large spacing. On the other hand the temperature distribution is not symmetrical around the centerline of the plate. Isothermal contours took the elliptical shape due to the effect of the interaction between the two jets. The elliptical shape is more significant as the jet spacing is increased. It was observed from Figs. 5–10 that the temperature decreases at the edges of plate as the jet spacing increases especially from strong jet side. This is due the domain area of the jet is increased by increasing the jet spacing. This provided more heat transfer rate.

6.2. Effect of Reynolds number on isothermal contours

The effect of Reynolds number on the temperature distribution was shown also from Figs. 5–10. At fixed jet-to-jet spacing, the isothermal Contours of the higher Reynolds number are dominated than for the lower Reynolds number left jet. For the same jet-to-jet spacing increasing the right Reynolds number more than the left decreases the wall temperature. It is more significant from Figs. 5–7 where the Reynolds number of the left jet was fixed at 7100 while the right increased from 15,400 to 30,800 that the isothermal contours took the shape of two pulleys with belt. The smaller pulley presented the low Reynolds number.

6.3. Effect of jet spacing on local Nusselt number

The effect of Jet Spacing on local Nusselt is shown in Fig. 11 for different Reynolds numbers and dimensionless jet-to-jet. It is observed that the stagnation zone changed for different dimensionless jet-to-jet spacing. Increasing the jet-to-jet spacing increases the local Nusselt number. Isotherms are near to each other causing high temperature gradient causing a high local Nusselt number whereas in the interaction zone isotherms are far away from each other reducing the temperature gradient and consequently reduced Nusselt number. Increasing the jet spacing decreases the wall temperature far from the center line of the plate.

6.4. Effect of Reynolds number on local Nusselt number

Fig. 12 shows the effect of increasing the Reynolds number of both jets on the local Nusselt number. The local Nusselt number is plotted for the dimensionless radius. The local Nusselt number plotted from the dimensionless radius is bigger than value 11.36, as it is the stagnation point for each jet. The local Nusselt is plotted for the case of $X/dj = 22.73$. The local Nusselt number increases as the Reynolds number of the right het increases while fixing the other at constant value. The local number decreases sharply as the dimensionless radius increases to a value where the hydraulic jump occurs then the decrease is stepper as the water velocity is decreased.

6.5. Effect of jet spacing on average Nusselt number

The average Nusselt number is plotted for dimensionless jet spacing for different Reynolds number. Fig. 13 shows the effect of the interaction on the average local Nusselt for dimensionless radius. As the dimensionless jet spacing increases the average local Nusselt number increases. For the same dimensionless jet spacing increasing the dimensionless radius, the average local Nusselt number decreases.

6.6. Effect of Reynolds number on average Nusselt number

Fig. 14 shows the effect of increasing the Reynolds number of both jets on the average Local Nusselt number at fixed dimensionless jet spacing at 22.27. The same observation as in the local Nusselt number. Increasing the Reynolds number increases the water film velocity and decreases the wall temperature as showed in the temperature wall distribution. From Fig. 14a shows the effect of increasing right Reynolds number while the left Reynolds number is fixed at constant value. The average Nusselt increased as the right Reynolds number increased. Comparing between the two Fig. 14a with

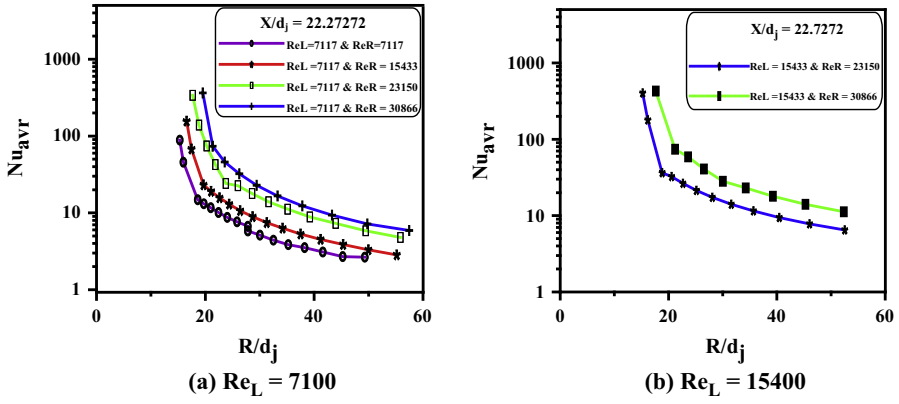

Figure 14 Effect of Reynolds number on average local Nusselt number.

Fig. 14b, increasing the Reynolds number for both jets increases the average Nusselt number more significantly where the water velocity from the two jets increased tending to decrease the wall temperature as the turbulence increases.

6.7. *Combined effect of Reynolds number and jets spacing on dimensionless water film thickness distribution*

The film thickness has a very important effect on the rate of heat transfer and the value of local Nusselt number. As the film thickness is increased the water velocity in the plate direction decreases. The reduction in velocity reduces the value of local Nusselt number. Fig. 15 represented the dimensionless water film thickness for different Reynolds number for the two jets at various dimensionless jet spacing. It is seen the dimensionless film thickness is very small in the two jets area. In these areas the water velocity is very high compared with the other regions. Therefore the rate of heat transfer in these areas is very high. As we move from one jet directed to the other jet, the film thickness slightly increases. Until the two streams of water reach each other collusions occur between the two streams. This location is called the interference zone. It is seen that, the dimensionless film thickness increases rapidly at interference zone. In the case of small jet spacing, the film thickness

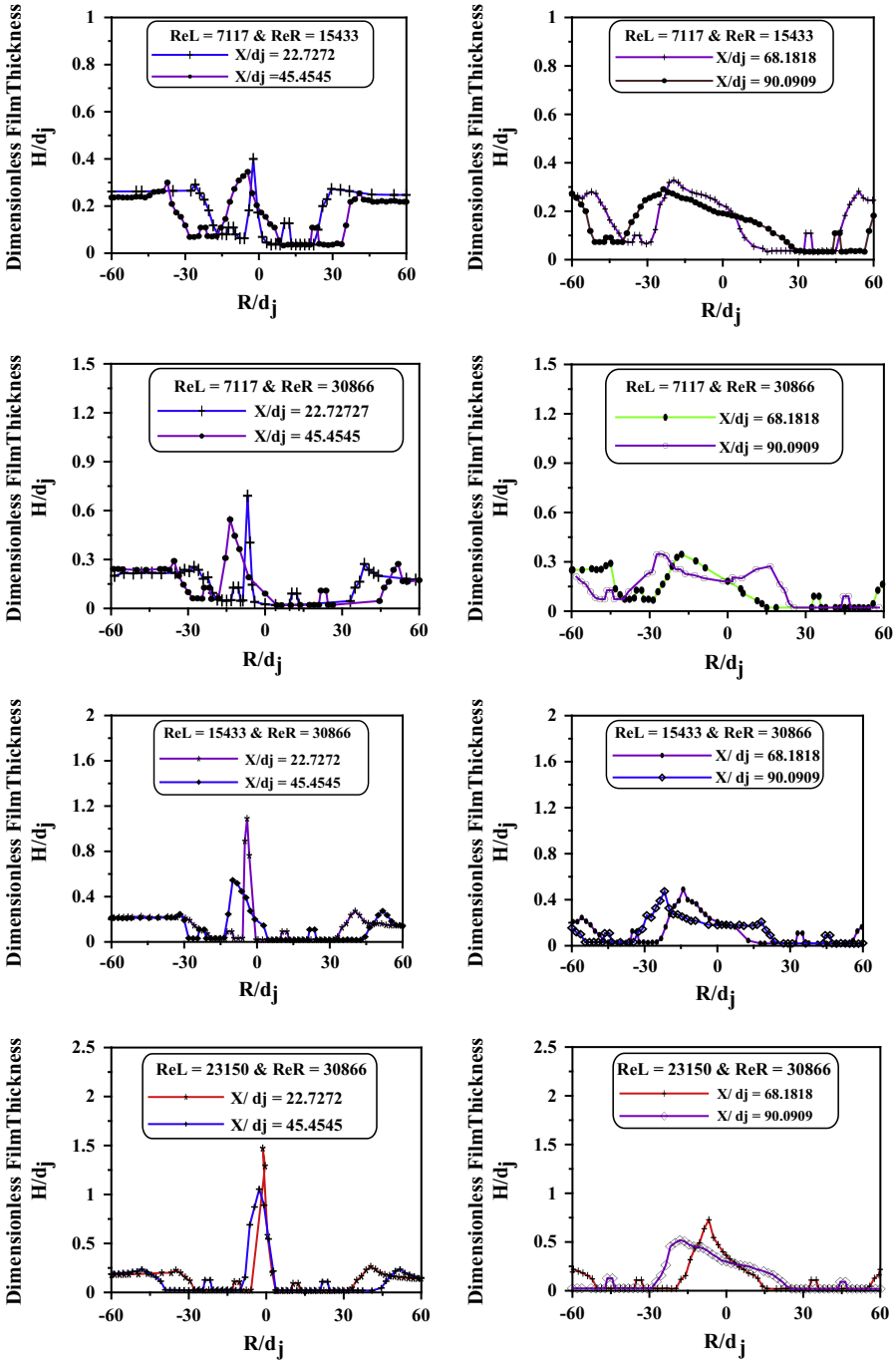

Figure 15 Combined effect of Reynolds number and jets spacing on dimensionless water film thickness distribution.

at the interference region increases dramatically by increasing the jet Reynolds number of the left jet. The dimensionless film thickness increases from 0.42 to 1.5 as the left jet Reynolds increases from 7100 to 23,150. The increase in the film thickness reduces the local Nusselt number. It is also noticed that, as increasing the dimensionless jet-to-jet spacing, the dimensionless film thickness decreased and the area of the interaction between the two jets increased. The location of the maximum dimensionless film thickness increased more toward the weaker Reynolds number jet. As the jet spacing increased the jets domain increases and the water velocity in the plat direction is decreased. This reduces the impact force due to the collision of the two streams. Therefore the dimensionless film thickness at the interference zone decreases as the distance between the two jets is increased. The water velocity for the stronger jet is higher than that for weaker jet. Therefore the location of the interference zone is shifted more to the weaker jet. As the jet Reynolds number for the weaker jet increases the location of the interference zone is shifted to the direction of the stronger jet. If the jets Reynolds number is equal the interference zone lies at midpoint between the two jets. The interference zone is much narrower in small jet spacing. On the other hand, the interference zone is thicker in the case of high jet spacing.

7. Conclusions

The hydrodynamic and the thermal characterizations of double impinging circular jets are analyzed. The effects of increasing the Reynolds number and the jet spacing on temperature distribution, as well as local and average local Nusselt numbers were studied. The Nusselt number values are very high at the jet regions. In these areas the film thickness is very small and this leads to a very high radial velocity causing the values of Nusselt number to be higher than one thousand. Therefore, these areas can be considered as super cooling areas. As we move away from the jet regions, the interaction between the flows from the two jets increases the water film thickness which reduces the value of radial velocity leading to a reduction in the value of Nusselt number. The temperature distribution shows elliptical shape due to the effects of both Reynolds number and the jet spacing. The experimental results showed clearly that the effect of increasing the Reynolds numbers for one jet than the other increases the local and average local Nusselt numbers for the same dimensionless jet-to-jet spacing as the water velocity increases. Also increasing the jet-to-jet spacing increases both the local and average local Nusselt numbers. The film thickness was measured for different dimensionless radii. Increasing the Reynolds number increases the water film thickness at the interaction zone causing turbulence. The water film thickness decreases as the jet spacing increases and the water velocity decreases.

References

[1] E.J. Watson, The radial spread of a liquid jet over a horizontal plane, J. Fluid Mech. 20 (1964) 481–499.

[2] Z.H. Chaudhury, Heat transfer in Radial liquid jet, J. Fluid Mech. 20 (1964) 501–511.

[3] A.D.D. Craik, R.C. Latham, M.J. Fawkes, P.W.F. Gribbon, The circular hydraulic jump, J. Fluid Mech. 112 (1981) 347–362.

[4] D.T. Vader, F.P. Incropera, R. Viskanta, Local convective heat transfers from a heated Surface to an impinging planner jet of water, Int. J. Heat Mass Transfer 34 (1991) 611–623.

[5] O. Zeiton, Convective heat transfer in the presence of a free surface, M.Sc. Thesis. Dept. of Mechanical Engineering, University of Alexandria, Alexandria, Egypt, 1988.

[6] M.A. Teamah, S. Farahat, Experimental and numerical heat transfer from impinging of single free liquid jet, Alexandria Eng. J. 42 (2003) 559–575.

[7] M.A. Teamah, S. Farahat, Experimental heat transfer due to impinging of water from multiple jets on a heated surface, Alexandria Eng. J. 45 (2006) 1–13.

[8] E.N. Wang, L. Zhang, L. Jiang, Micro-machined jets for liquid impingement cooling of VLSI chips, J. Microelectro Mech. Syst. 13 (2004) 833–842.

[9] M. Fabbri, S. Jiang, V.K. Dhir, Experimental investigation of single-phase Micro Jets impingement cooling for electronic applications, in: Proceeding of Heat Transfer Conference, Las Vegas, Nevada, 2003.

[10] J. Stevens, B.W. Webb, Local heat transfers coefficients under an ax symmetric, single-phase liquid jet, J. Heat Transfer 112 (1991) 71–78.

[11] J. Stevens, B.W. Webb, The effect of inclination on local heat transfer under an ax symmetric free liquid jet, Int. J. Heat Mass Transfer 34 (1991) 1227–1236.

[12] M. Gradeck, A. Kouachi, A. Dani, Experimental and numerical study of the hydraulic jump of an impinging jets on a moving surface, Exp. Thermal Fluid Sci. 30 (2006) 193–201.

[13] Y.C. Chen, C.F. Ma, Z.X. Yuan, Heat transfer enhancement with impinging free surface liquid jets flowing over heated wall coated by a ferro fluid, Int. J. Heat Mass Transfer 44 (2001) 499–502.

[14] S.J. Slayzak, R. Viskanta, F.P. Incropera, Effects of interaction between adjacent free surface planner on local heat transfer from the Impingement Surface, Int. J. Heat Mass Transfer 37 (1994) 269–282.

[15] J.H. Lienhard, Heat transfer by impingement of circular free-surface liquid Jets, in: 18th National Conference Heat and Mass Transfer IIT, Guwahati, India, 2006.

[16] H. Sun, C.F. Ma, Y.C. Chen, Prandtl number dependence of impingement heat transfer with circular free-surface liquid jets, Int. J. Heat Mass Transfer 41 (1998) 1360–1363.

[17] X.S. Wang, Z. Dagan, L.M. JIJI, Heat transfer between a circular free Impinging jet and a solid surface with non-uniform wall temperature or wall Heat flux-1. Solution for the stagnation region, Int. J. Heat Mass Transfer 32 (1989) 1351–1360.

[18] C.F. Ma, Q. Zheng, S.Y. Ko, Local heat transfer and recovery factor with the impinging free-surface circular jets of transformer oil, Int. J. Heat Mass Transfer 40 (1997) 4295–4308.

[19] S. Ishigai, S. Nakanishi, M. Mizuno, T. Imaura, Heat transfer of the impinging round water in the interference zone of film flow along the wall, JSME 20 (1977) 85–92.

[20] M.A. Teamah, M.K. Ibrahim, M.M. Khairat Dawood, E. Abdel Aleem, Experimental investigation for hydrodynamic flow due to obliquely free circular water jet impinging on horizontal flat plate, Eur. J. Sci. Res. 83 (1) (2012) 60–75.

[21] A. Malvandi, F. Hedayati, D.D. Ganji, Thermodynamic optimization of fluid flow over an isothermal moving plate, Alexandria Eng. J. 52 (3) (2013) 277–283.

[22] Kalidas Das, Flow and heat transfer characteristics of nanofluids in a rotating frame, Alexandria Eng. J. 53 (3) (2014) 757–766.

[23] T. Hayat, M. Qasim, S.A. Shehzad, A. Alsaedi, Unsteady stagnation point flow of second grade fluid with variable free stream, Alexandria Eng. J. 53 (2) (2014) 455–461.

[24] G. Nasif, R.M. Barron, R. Balachandar, Simulation of jet impingement heat transfer onto a moving disc, Int. J. Heat Mass Transf. 80 (2015) 539–550.

[25] F.M. White, Fluid Mechanics, fifth ed., McGraw-Hill, 2003.